

Improved refined plastic hinge analysis accounting for local buckling and lateral-torsional buckling

Huu-Tai Thai^{1,2a}, Seung-Eock Kim^{2b} and Jongmin Kim^{*2}

¹ School of Engineering and Mathematical Sciences, La Trobe University, Bundoora, VIC 3086, Australia

² Department of Civil and Environmental Engineering, Sejong University, 209 Neungdong-ro, Gwangjin-gu, Seoul 05006, Republic of Korea

(Received August 04, 2016, Revised March 06, 2017, Accepted April 07, 2017)

Abstract. In this paper, a conventional refined plastic hinge analysis is improved to account for the effects of local buckling and lateral-torsional buckling. The degradation of flexural strength caused by these effects is implicitly considered using practical LRFD equation. The second-order effect is captured using stability functions to minimize modeling and solution time. An incremental-iterative scheme based on the generalized displacement control method is employed to solve the nonlinear equilibrium equations. A computer program is developed to predict the second-order inelastic behavior of space steel frames. To verify the accuracy and efficiency of the proposed program, the obtained results are compared with the existing results and those generated using the commercial finite element package ABAQUS. It can be concluded that the proposed program proves to be a reliable and effective tool for daily use in engineering design.

Keywords: stability function; plastic hinge; local buckling; lateral-torsional buckling; generalized displacement control method

1. Introduction

In recent years, the nonlinear inelastic analysis of space steel frames has been studied extensively by utilizing two different approaches of finite element and beam-column. In the finite element method, interpolation functions are adopted to represent the second-order effects, and fiber model is used to capture the spread of plasticity (Teh and Clarke 1999, Torkamani and Sonmez 2001, Jiang *et al.* 2002, Jiang and Usmani 2013, Rigobello *et al.* 2013, Zubydan 2013). Although the solution of this method can be considered to be accurate, it has not been applied widely for daily use in design because of its highly computational cost. In the beam-column approach, stability functions derived from the differential equilibrium equation are employed to capture the second-order effects, and refined plastic hinge model is adopted to account for the inelastic behavior (Kim *et al.* 2001, Iu *et al.* 2009, Thai and Kim 2011, Landesmann 2012, Liu *et al.* 2012, Chiorean 2013, Thai and Choi 2013). The benefit of this method is that it enables only one or two elements per member to accurately predict the nonlinear response of structures and, hence, to save computational time.

The local buckling and lateral-torsional buckling are important factors that should be considered in structural steel design. These types of instability phenomena occur

when a structural member undergoes significant out-of-

plane bending and twisting or width-thickness ratio. The effects of local buckling and lateral-torsional buckling can be considered by either the application of Standards (Hoang and Nguyen Dang 2008) or the analysis (Mohri *et al.* 2008). It is well known that the load pattern, end condition and unbraced length have a considerable effect on the lateral-torsional buckling of a beam. Significant research has been done to evaluate the effect of the location of the applied load on the lateral-torsional buckling of a beam. It is found that applying the load at a location below the shear centre is more stable than applying the load above the shear centre. Since the proposed analysis aims to determine only the ultimate strength of the whole structural system rather than to examine the local buckling and lateral-torsional buckling behaviors of a component member, the use of code formulae is deemed appropriate for tracing the nonlinear behavior of the frame including local buckling and lateral-torsional buckling effects. In present work, these effects are implicitly accounted for using the LRFD Specification (AISC-LRFD 1994). According to LRFD, the nominal flexural strength is the lowest value obtained according to the limit stress of: (a) yielding; (b) local buckling; and (c) lateral-torsional buckling. The local buckling strength depends on the width-thickness ratio of a section, while the lateral-torsional buckling strength relies on the unbraced length, cross-sectional shape and material properties.

Since the conventional refined plastic hinge analysis ignored the local buckling and lateral-torsional buckling effects by assuming compact section and adequate lateral bracing, improvement of the refined plastic hinge analysis was made by accounting for only local buckling (Kim *et al.* 2003) or lateral-torsional buckling (Kim *et al.* 2002).

*Corresponding author, Assistant Professor,

E-mail: jongmin@sejong.ac.kr

^a Senior Lecturer, E-mail: tai.thai@latrobe.edu.au

^b Professor, E-mail: sekim@sejong.ac.kr

However, for a member with intermediate length, the combined failure mode of local buckling and lateral-torsional buckling is obtained. Therefore, the refined plastic hinge model should be improved to account for both local buckling and lateral-torsional buckling.

The purpose of this paper is to improve the refined plastic hinge analysis by accounting for both local buckling and lateral-torsional buckling effects. The second-order effects are accurately captured using the stability functions, while the inelastic effects are considered using the refined plastic hinge model. The degradation of the flexural strength caused by local buckling and lateral-torsional buckling is implicitly accounted for using the practical LRFD equation. To trace the descending branch of an equilibrium path, the Generalized Displacement Control (GDC) method proposed by Yang and Shieh (1990) is employed for solving the nonlinear equilibrium equations. This algorithm can accurately trace the equilibrium path of nonlinear problems with multiple limit points and snap-back points as demonstrated in numerical examples. The bowing and warping effects are not considered in this study. A computer program is developed. Several numerical examples are presented to show the accuracy and computational efficiency of the proposed program in predicting the second-order inelastic behavior of space steel frames.

2. Formulation

2.1 Stability functions accounting for second-order effects

To capture the effect of the interaction between axial force and bending moment, the stability functions are used to minimize modeling and solution time. From Kim *et al.* (2001), the incremental form of member basic force and deformation relationship of space beam-column element can be expressed as

$$\begin{Bmatrix} P \\ M_{yA} \\ M_{yB} \\ M_{zA} \\ M_{zB} \\ T \end{Bmatrix} = \begin{bmatrix} \frac{EA}{L} & 0 & 0 & 0 & 0 & 0 \\ 0 & S_{1y} \frac{EI_y}{L} & S_{2y} \frac{EI_y}{L} & 0 & 0 & 0 \\ 0 & S_{2y} \frac{EI_y}{L} & S_{1y} \frac{EI_y}{L} & 0 & 0 & 0 \\ 0 & 0 & 0 & S_{1z} \frac{EI_z}{L} & S_{2z} \frac{EI_z}{L} & 0 \\ 0 & 0 & 0 & S_{2z} \frac{EI_z}{L} & S_{1z} \frac{EI_z}{L} & 0 \\ 0 & 0 & 0 & 0 & 0 & \frac{GJ}{L} \end{bmatrix} \begin{Bmatrix} \delta \\ \theta_{yA} \\ \theta_{yB} \\ \theta_{zA} \\ \theta_{zB} \\ \phi \end{Bmatrix} \quad (1)$$

where P , M_{yA} , M_{yB} , M_{zA} , M_{zB} , and T are incremental axial force, end moments with respect to y and z axes, and torsion, respectively; δ , θ_{yA} , θ_{yB} , θ_{zA} , θ_{zB} , and ϕ are the incremental axial displacement, the joint rotations, and the angle of twist; A , I_y , I_z , J and L are area, moment of inertia with respect to y and z axes, torsional constant, and length of beam-column element; E and G are elastic and shear modulus of material; S_{1n} and S_{2n} are the stability functions with respect to n axis ($n = y, z$) given as

$$S_{1n} = \begin{cases} \frac{\pi\sqrt{\rho_n} \sin(\pi\sqrt{\rho_n}) - \pi^2\rho_n \cos(\pi\sqrt{\rho_n})}{2 - 2\cos(\pi\sqrt{\rho_n}) - \pi\sqrt{\rho_n} \sin(\pi\sqrt{\rho_n})} & \text{if } P < 0 \\ \frac{\pi^2\rho_n \cosh(\pi\sqrt{\rho_n}) - \pi\sqrt{\rho_n} \sinh(\pi\sqrt{\rho_n})}{2 - 2\cosh(\pi\sqrt{\rho_n}) + \pi\sqrt{\rho_n} \sinh(\pi\sqrt{\rho_n})} & \text{if } P > 0 \end{cases} \quad (2a)$$

$$S_{2n} = \begin{cases} \frac{\pi^2\rho_n - \pi\sqrt{\rho_n} \sin(\pi\sqrt{\rho_n})}{2 - 2\cos(\pi\sqrt{\rho_n}) - \pi\sqrt{\rho_n} \sin(\pi\sqrt{\rho_n})} & \text{if } P < 0 \\ \frac{\pi\sqrt{\rho_n} \sinh(\pi\sqrt{\rho_n}) - \pi^2\rho_n}{2 - 2\cosh(\pi\sqrt{\rho_n}) + \pi\sqrt{\rho_n} \sinh(\pi\sqrt{\rho_n})} & \text{if } P > 0 \end{cases} \quad (2b)$$

where $\rho_n = |P|/(\pi^2 EI_n/L^2)$.

2.2 Refined plastic hinge model accounting for inelastic effects

The material nonlinearity includes gradual yielding of steel associated with residual stresses and flexure. The gradual yielding due to residual stresses is considered by utilizing the Column Research Council (CRC) tangent modulus concept E_t , while the gradual yielding due to flexure is represented by the parabolic function. The relationship between basic force and deformation of space beam-column is modified to account for the inelastic effects as

$$\begin{Bmatrix} P \\ M_{yA} \\ M_{yB} \\ M_{zA} \\ M_{zB} \\ T \end{Bmatrix} = \begin{bmatrix} E_t A/L & 0 & 0 & 0 & 0 \\ 0 & k_{iyy} & k_{ijy} & 0 & 0 \\ 0 & k_{jyy} & k_{jyy} & 0 & 0 \\ 0 & 0 & 0 & k_{iiz} & k_{ijz} \\ 0 & 0 & 0 & k_{jiz} & k_{jiz} \\ 0 & 0 & 0 & 0 & GJ/L \end{bmatrix} \begin{Bmatrix} \delta \\ \theta_{yA} \\ \theta_{yB} \\ \theta_{zA} \\ \theta_{zB} \\ \phi \end{Bmatrix} \quad (3)$$

where

$$k_{iyy} = \eta_A \left(S_1 - \frac{S_2^2}{S_1} (1 - \eta_B) \right) \frac{E_t I_y}{L} \quad (4a)$$

$$k_{ijy} = \eta_A \eta_B S_2 \frac{E_t I_y}{L} \quad (4b)$$

$$k_{jyy} = \eta_B \left(S_1 - \frac{S_2^2}{S_1} (1 - \eta_A) \right) \frac{E_t I_y}{L} \quad (4c)$$

$$k_{iiz} = \eta_A \left(S_3 - \frac{S_4^2}{S_3} (1 - \eta_B) \right) \frac{E_t I_z}{L} \quad (4d)$$

$$k_{ijz} = \eta_A \eta_B S_4 \frac{E_t I_z}{L} \quad (4e)$$

$$k_{jiz} = \eta_B \left(S_3 - \frac{S_4^2}{S_3} (1 - \eta_A) \right) \frac{E_t I_z}{L} \quad (4f)$$

The terms η_A and η_B are scalar parameters that allow for gradual inelastic stiffness reduction of the element

associated with plastification at ends A and B. These terms are equal to 1.0 when the element is elastic, and zero when a plastic hinge is formed. The parameter η is assumed to vary according to the parabolic function as

$$\eta = 1.0 \quad \text{or} \quad \alpha \leq 0.5 \quad (5a)$$

$$\eta = 4\alpha(1-\alpha) \quad \text{for} \quad \alpha > 0.5 \quad (5b)$$

where α can be expressed in yield surface proposed by Orbison (1982) as

$$\alpha = 1.15p^2 + m_z^2 + m_y^4 + 3.67p^2m_z^2 + 3.0p^6m_y^2 + 4.65m_z^4m_y^2 \quad (6)$$

where

$$p = P/P_y \quad (7a)$$

$$m_y = M_y/M_{py} \quad \text{for weak axis} \quad (7b)$$

$$m_z = M_z/M_{pz} \quad \text{for strong axis} \quad (7c)$$

2.3 Shear deformation effect

To account for the shear deformation effect, the member basic force and deformation relationship of space beam-column is modified as follows

$$\begin{Bmatrix} P \\ M_{yA} \\ M_{yB} \\ M_{zA} \\ M_{zB} \\ T \end{Bmatrix} = \begin{bmatrix} \frac{E_t A}{L} & 0 & 0 & 0 & 0 & 0 \\ 0 & C_{iyy} & C_{ijy} & 0 & 0 & 0 \\ 0 & C_{ijy} & C_{jyy} & 0 & 0 & 0 \\ 0 & 0 & 0 & C_{iiz} & C_{ijz} & 0 \\ 0 & 0 & 0 & C_{ijz} & C_{jiz} & 0 \\ 0 & 0 & 0 & 0 & 0 & \frac{GJ}{L} \end{bmatrix} \begin{Bmatrix} \delta \\ \theta_{yA} \\ \theta_{yB} \\ \theta_{zA} \\ \theta_{zB} \\ \phi \end{Bmatrix} \quad (8)$$

where

$$C_{iyy} = \frac{k_{iy}k_{jyy} - k_{ijy}^2 + k_{iyy}A_{sz}GL}{k_{iyy} + k_{jyy} + 2k_{ijy} + A_{sz}GL} \quad (9a)$$

$$C_{ijy} = \frac{-k_{iyy}k_{jyy} + k_{ijy}^2 + k_{ijy}A_{sz}GL}{k_{iyy} + k_{jyy} + 2k_{ijy} + A_{sz}GL} \quad (9b)$$

$$C_{jyy} = \frac{k_{iy}k_{jyy} - k_{ijy}^2 + k_{jyy}A_{sz}GL}{k_{iyy} + k_{jyy} + 2k_{ijy} + A_{sz}GL} \quad (9c)$$

$$C_{iiz} = \frac{k_{iz}k_{jz} - k_{ijz}^2 + k_{iiz}A_{sy}GL}{k_{iiz} + k_{jz} + 2k_{ijz} + A_{sy}GL} \quad (9d)$$

$$C_{ijz} = \frac{-k_{iiz}k_{jz} + k_{ijz}^2 + k_{ijz}A_{sy}GL}{k_{iiz} + k_{jz} + 2k_{ijz} + A_{sy}GL} \quad (9e)$$

$$C_{jiz} = \frac{k_{iz}k_{jz} - k_{ijz}^2 + k_{jiz}A_{sy}GL}{k_{iiz} + k_{jz} + 2k_{ijz} + A_{sy}GL} \quad (9f)$$

where A_{sy} and A_{sz} are the shear areas with respect to y and z axes, respectively.

2.4 Local buckling effect

When the width-thickness ratio of a section is greater than a limit, local buckling of a flange or web will occur as the applied load increases. The local buckling causes the degradation of the flexural strength. The width-thickness ratio λ of the flange and web is an important factor influencing the local buckling strength of I-shaped sections. In this study, the local buckling strength M_{n1} is determined from LRFD equation as

$$M_{n1} = M_p \quad \text{for} \quad \lambda < \lambda_p \quad (10a)$$

$$M_{n1} = M_p - (M_p - M_r) \left(\frac{\lambda - \lambda_p}{\lambda_r - \lambda_p} \right) \quad \text{for} \quad \lambda_p \leq \lambda \leq \lambda_r \quad (10b)$$

$$M_{n1} = M_{cr} = S_x F_{cr} \leq M_p \quad \text{for} \quad \lambda > \lambda_r \quad (10c)$$

The notations of Eq. (10) are defined in Table 1. When λ of the web is greater than λ_r , the flexural strength is given by

$$M_{n1} = S_x R_{PG} F_{cr} \quad (11)$$

where the reduction factor R_{PG} is expressed as

$$R_{PG} = 1 - \frac{a_r}{1200 + 300a_r} \left(\frac{h_c}{t_w} - \frac{970}{\sqrt{F_{cr}}} \right) \leq 1.0 \quad (12)$$

where $a_r = A_w/A_f \leq 10$; h_c = twice the distance from the centroid to the inside face of the compression flange.

2.5 Lateral-torsional buckling effect

When a member is bent about its major axis, the out-of-plane motion consisting of bending and twisting will occur as the applied load increases. The out-of-plane motion results in the degradation of the flexural strength and stiffness about its major axis. The unbraced length L_b , cross-sectional shape and material property are important factors influencing the lateral-torsional buckling strength. The lateral-torsional buckling strength M_{n2} is determined from the LRFD equation as

when $L_b < L_p$

$$M_{n2} = M_p \quad (13a)$$

when $L_p \leq L_b \leq L_r$

$$M_{n2} = C_b \left[M_p - (M_p - M_r) \left(\frac{L_b - L_p}{L_r - L_p} \right) \right] \quad (13b)$$

Table 1 Flexural strength and limit of width-thickness ratio for I-sections^a (unit: kip-in)

Item	Flange buckling	Web buckling
M_p	$F_y Z$	$F_y Z$
M_r	$F_L S_x$	$F_y S_x$
F_{cr}	$\begin{cases} \frac{20,000}{\lambda^2} & \text{for rolled shape} \\ \frac{26,200k_c}{\lambda^2} & \text{for welded shape} \end{cases}$	$\begin{cases} F_y & \text{for } \lambda < \lambda_p \\ F_y \left[1 - \frac{1}{2} \left(\frac{\lambda - \lambda_p}{\lambda_r - \lambda_p} \right) \right] & \text{for } \lambda_p \leq \lambda \leq \lambda_r \\ C_{PG} / \lambda^2 & \text{for } \lambda > \lambda_r \end{cases}$
λ	$b_f / 2t_f$	h / t_w
λ_p	$\frac{65}{\sqrt{F_y}}$	$\begin{cases} \frac{640}{\sqrt{F_y}} \left(1 - \frac{2.75P_u}{\phi_b P_y} \right) & \text{for } \frac{P_u}{\phi_b P_y} \leq 0.125 \\ \frac{191}{\sqrt{F_y}} \left(2.33 - \frac{P_u}{\phi_b P_y} \right) \geq \frac{253}{\sqrt{F_y}} & \text{for } \frac{P_u}{\phi_b P_y} > 0.125 \end{cases}$
λ_r	$\begin{cases} \frac{162}{\sqrt{F_L / k_c}} & \text{for rolled shape} \\ \frac{141}{\sqrt{F_L}} & \text{for welded shape} \end{cases}$	$\frac{970}{\sqrt{F_y}} \left(1 - \frac{0.74P_u}{\phi_b P_y} \right)$

^a where S_x = elastic section modulus about major axis; $F_L = F_y - F_R$, F_y = specified minimum yield stress, F_R = compressive residual stress in flange equal to 10 ksi for rolled shapes and 16.5 ksi for welded shapes; b_f = flange width, t_f = flange thickness, t_w = web thickness; h = depth of web, $\phi_b = 0.9$, $k_c = 4 / \sqrt{h / t_w}$ and $0.35 \leq k_c \leq 0.763$, and $C_{PG} = 260,200k_c$

when $L_b > L_r$

$$M_{n2} = \begin{cases} C_b \frac{\pi}{L_u} \sqrt{EI_y GJ + \left(\frac{\pi E}{L_u} \right)^2 I_y C_w} & \text{for I-shaped and channel sections} \\ \frac{57,000 C_b \sqrt{JA}}{L_u / r_y} & \text{for box and solid rectangular sections} \end{cases} \quad (13c)$$

where M_p and M_r are given in Table 1; C_w is the warping constant; L_p and L_r are the limiting unbraced plastic and elastic lengths, respectively, determined as follows

$$L_p = \begin{cases} \frac{300r_y}{\sqrt{F_y}} & \text{for I-shaped and channel sections} \\ \frac{3,750r_y}{M_p} \sqrt{JA} & \text{for box and solid rectangular sections} \end{cases} \quad (14)$$

$$L_r = \begin{cases} \frac{r_y X_1}{F_L} \sqrt{1 + X_2 F_L^2} & \text{for I-shaped and channel sections} \\ \frac{57,000r_y}{M_r} \sqrt{JA} & \text{for box and solid rectangular sections} \end{cases} \quad (15)$$

where

$$X_1 = \frac{\pi}{S_x} \sqrt{\frac{EGJA}{2}} \quad (16)$$

$$X_2 = 4 \frac{C_w}{I_y} \left(\frac{S_x}{GJ} \right)^2 \quad (17)$$

in which r_y is the radius of gyration of the section about the weak axis; S_x , F_y and F_L are given in Table 1. C_b is a modification for non-uniform moment diagrams. The physical meaning of C_b is that it represents the amount of an increase in load-carrying capacity when compared with the critical uniform loading case. An empirical formula for C_b is expressed as

$$C_b = \frac{12.5M_{\max}}{2.5M_{\max} + 3M_A + 4M_B + 3M_C} \quad (18)$$

where M_{\max} is absolute value of maximum moment in the unbraced segment, sum of moments in sway and non-sway cases; M_A is the absolute value of moment at quarter point of the unbraced segment, sum of moments in sway and non-sway cases; M_B is the absolute value of moment at centerline of the unbraced segment, sum of moments in sway and non-sway cases; M_C is the absolute value of moment at three quarter point of the unbraced segment, sum of moments in sway and non-sway cases. If the local buckling and lateral-torsional buckling are considered, the plastic moment M_{pz} in Eq. (7c) is replaced by the buckling strength M_n given as

$$M_n = \min(M_{n1}, M_{n2}) \quad (19)$$

2.6 Modeling of element stiffness after buckling

When a member reaches its local buckling or lateral-torsional buckling strength M_n indicated in Eq. (19), the moment of inertia of the member is assumed to be zero so that the inelastic moment redistribution is not allowed for

the member. This approximation is deemed appropriate for tracing the nonlinear behavior of the frame including local buckling and lateral-torsional buckling effects because the proposed analysis aims to determine only the ultimate strength of the whole structural system rather than to examine the local buckling and lateral-torsional buckling behaviors of a component member.

3. Nonlinear solution techniques

In this section, a numerical procedure for solving the nonlinear equations is presented based on the GDC method. The incremental form of equilibrium equation of structure can be rewritten for the j th iteration of the i th incremental step as

$$[K_{j-1}^i] \{\Delta D_j^i\} = \lambda_j^i \{\hat{P}\} + \{R_{j-1}^i\} \quad (20)$$

where $[K_{j-1}^i]$ is the tangent stiffness matrix, $\{\Delta D_j^i\}$ is the displacement increment vector, $\{\hat{P}\}$ is the reference load vector, $\{R_{j-1}^i\}$ is the unbalanced force vector, and λ_j^i is the load increment parameter.

Eq. (20) can be decomposed into the following equations

$$[K_{j-1}^i] \{\Delta \hat{D}_j^i\} = \{\hat{P}\} \quad (21)$$

$$[K_{j-1}^i] \{\Delta \bar{D}_j^i\} = \{R_{j-1}^i\} \quad (22)$$

$$\{\Delta D_j^i\} = \lambda_j^i \{\Delta \hat{D}_j^i\} + \{\Delta \bar{D}_j^i\} \quad (23)$$

Once the displacement increment vector $\{\Delta D_j^i\}$ is determined, the total displacement vector $\{D_j^i\}$ at the end of j th iteration can be accumulated as

$$\{D_j^i\} = \{D_{j-1}^i\} + \{\Delta D_j^i\} \quad (24)$$

The total applied load vector $\{P_j^i\}$ at the j th iteration of the i th incremental step relates to the reference load vector $\{\hat{P}\}$ as

$$\{P_j^i\} = \Lambda_j^i \{\hat{P}\} \quad (25)$$

where the load factor Λ_j^i can be related to the load increment parameter λ_j^i by

$$\Lambda_j^i = \Lambda_{j-1}^i + \lambda_j^i \quad (26)$$

The load increment parameter λ_j^i is an unknown. It is determined from a constraint condition. For the first iterative step ($j = 1$), the load increment parameter λ_j^i is determined based on the generalized stiffness parameter (GSP) as

$$\lambda_1^i = \lambda_1^1 \sqrt{GSP} \quad (27)$$

where λ_1^1 is an initial value of load increment parameter, and the GSP is defined as

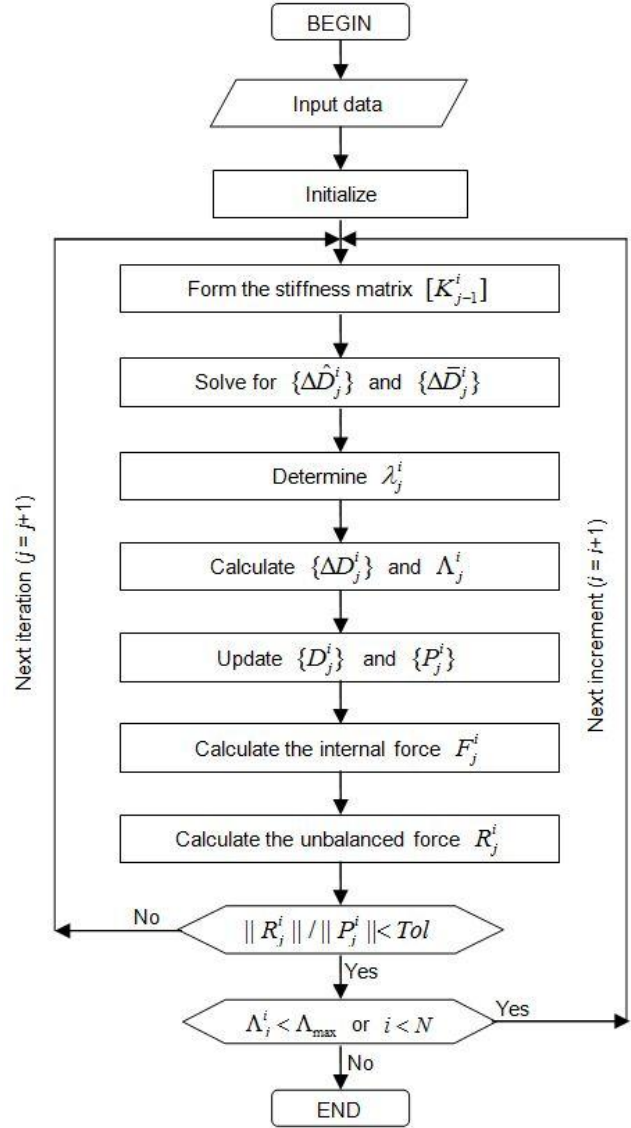


Fig. 1 Flow chart of the proposed program

$$GSP = \frac{\{\Delta \hat{D}_1^1\}^T \{\Delta \hat{D}_1^1\}}{\{\Delta \hat{D}_1^{i-1}\}^T \{\Delta \hat{D}_1^i\}} \quad (28)$$

For the iterative step ($j \geq 2$), the load increment parameter λ_j^i is calculated as

$$\lambda_j^i = - \frac{\{\Delta \hat{D}_1^{i-1}\}^T \{\Delta \bar{D}_j^i\}}{\{\Delta \hat{D}_1^{i-1}\}^T \{\Delta \hat{D}_j^i\}} \quad (29)$$

where $\{\Delta \hat{D}_1^{i-1}\}$ is the displacement increment generated by the reference load $\{\hat{P}\}$ at the first iteration of the previous ($i - 1$) incremental step, and $\{\Delta \bar{D}_j^i\}$ and $\{\Delta \hat{D}_j^i\}$ denote the displacement increments generated by the reference load and unbalanced force vectors, respectively, at the j th iteration of the i th incremental step, as defined in Eqs. (21)-(22).

4. Numerical examples

In this section, several numerical examples are presented and discussed to verify the accuracy and computational efficiency of the present study. A computer program written in FORTRAN is developed based on the above-mentioned algorithm for second-order inelastic analysis of space steel frames. A flow chart of the proposed program is illustrated in Fig. 1. For the verification purpose, the results obtained from present study are compared with those generated by ABAQUS and other available results reported in the literature. An elastic-perfectly plastic material model is used for all examples.

4.1 Cantilever beam

The cantilever beam as shown in Fig. 2 was analyzed by De Souza (2000) using force-based method with fiber model of the cross-section. The Young's modulus and Poisson ratio are $E = 200,000$ MPa and $\nu = 0.3$, respectively.

The load-displacement curves obtained by the proposed program are compared with those of De Souza (2000) and ABAQUS as shown in Fig. 3. The load-deflection curves obtained by the present study using four elements compare well with those given by De Souza with different values of yield stress. For the case of elastic response, ABAQUS can predict accurately the response using ten elements. However, for the inelastic case, if the beam is modeled as ten elements, discrepancy in the load-deflection curves

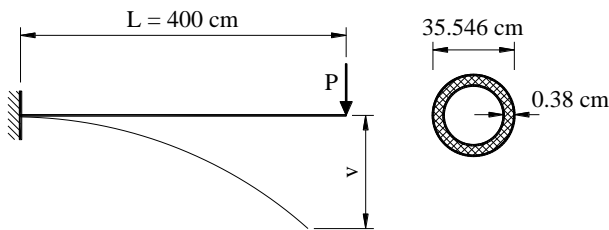


Fig. 2 Cantilever beam

generated by ABAQUS and the present study is quite obvious (Fig. 3). The discrepancy becomes small when fifty elements are used in the beam modeling. This example demonstrates the capability of the proposed program in capturing the large deflection inelastic behavior of structures.

4.2 Lee's frame

The next example deals with the snap-through and snap-back responses of the frame as shown in Fig. 4. Young's modulus, Poisson ratio and yield stress of the material are $E = 70,608$ MPa, $\nu = 0.3$ and $\sigma_y = 1,020$ MPa, respectively. This structure is employed to verify the capability of the proposed program in tracing the equilibrium path with multiple critical points. Each member is modeled using five and ten elements in proposed and ABAQUS programs, respectively.

The load-displacement curves predicted by the proposed program compare well with those of Cichon (1984) and ABAQUS as shown in Fig. 5. It can be seen that the proposed program can capture accurately the snap-through and snap-back responses of frames.

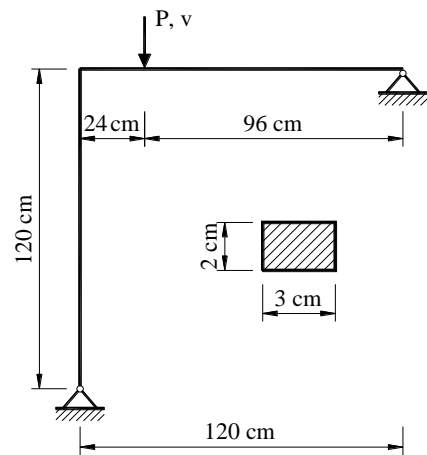


Fig. 4 Lee's frame

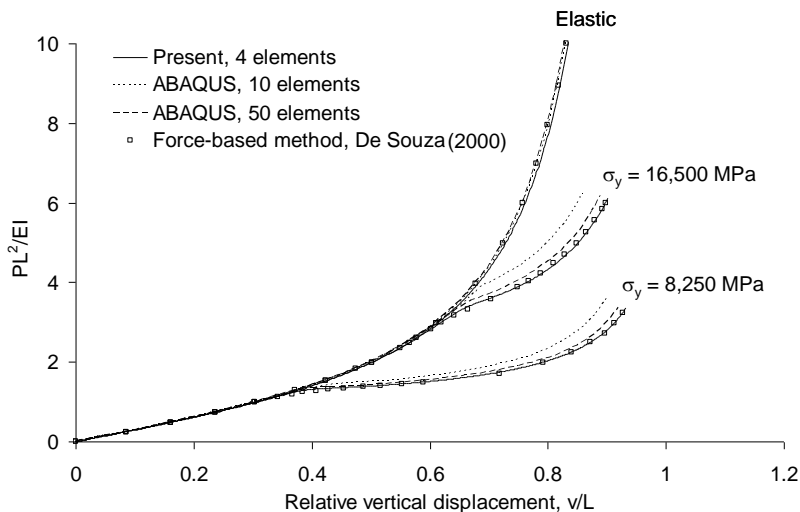


Fig. 3 Load-displacement curves of cantilever beam

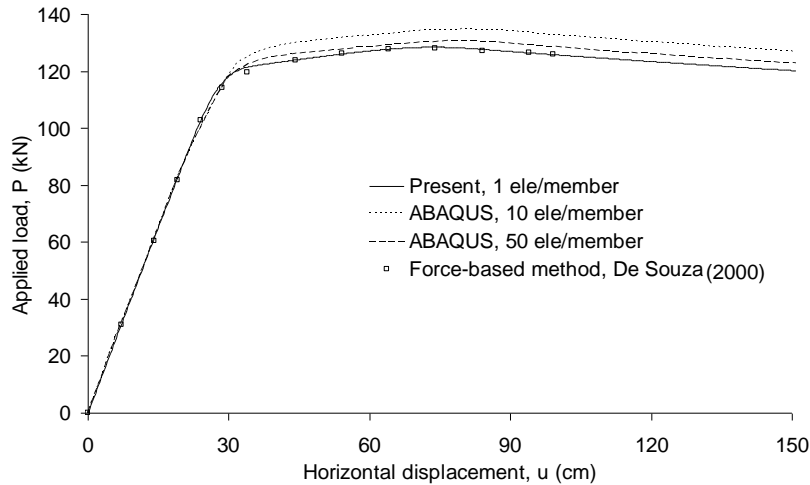


Fig. 7 Load-displacement curves of two-story space frame with rectangular sections

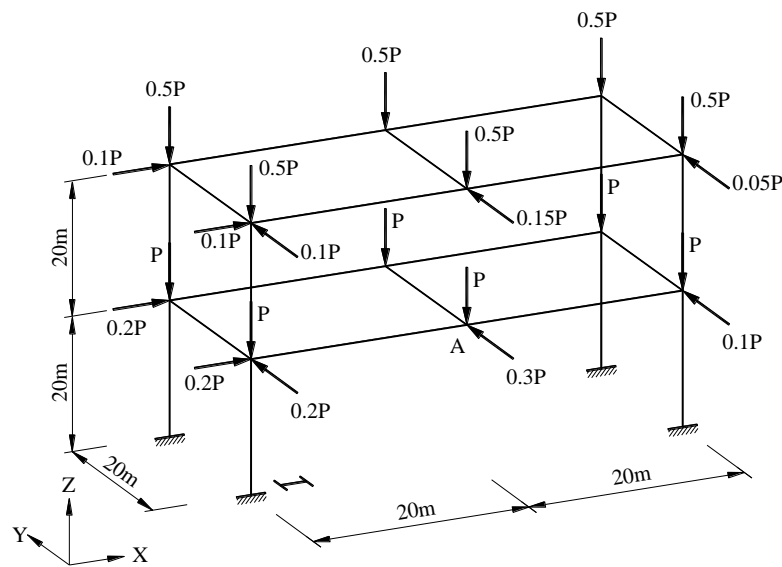


Fig. 8 Two-story space frame with I-shape sections

lateral-torsional buckling (LTB). Only one element per member is used to model the frame. Four analyses are compared in this example: (a) both LB and LTB considered (i.e., proposed analysis); (b) LB considered and LTB ignored; (c) LB ignored and LTB considered; and (d) both LB and LTB ignored (i.e., conventional refined plastic hinge analysis).

In the proposed analysis, the structure is collapsed by the combined failure mode of LB and LTB. The load-carrying capacity of the structural system is calculated to be 4.07 kN. If only LB is considered, the structural system is failed by the LB mode at the load-carrying capacity of 4.11 kN. If only LTB is considered, the structural system is failed by the LTB mode at the load-carrying capacity of 4.88 kN. If both LB and LTB are ignored (i.e., section develops full plastic moment capacity), the structural system is failed at the load-carrying capacity of 5.25 kN. As a result, the conventional refined plastic hinge analysis overpredicts the load-carrying capacity of the frame by 1.29 times. The load-displacement curves at node A in the Y-

direction generated by four analyses are compared in Fig. 9.

4.5 Twenty-story space frame

The twenty-story space steel frame shown in Fig. 10 was analyzed by Jiang *et al.* (2002) and Chiorean and Barsan (2005) using the mixed element and distributed plasticity methods, respectively. A50 steel with yield stress of 344.8 MPa and Young's modulus of 200,000 MPa is used for all sections. The load applied to the structure consists of gravity loads of 4.8 kN/m² and wind loads of 0.96 kN/m² acting in the Y-direction. These loads are converted into concentrated loads applied at the beam-column joints.

Jiang used both the plastic hinge and spread-of-plasticity elements to model this structure to shorten the computational time because the use of a full spread-of-plasticity analysis is very computationally intensive. When a member modeling by one plastic hinge element detected yielding to occur between the two ends, it was divided into eight spread-of-plasticity elements to accurately capture the

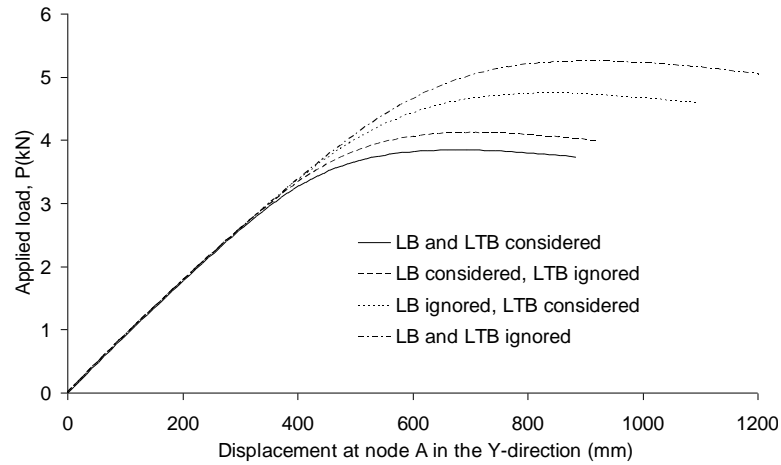


Fig. 9 Load-displacement curves of two-story space frame with I-shape sections

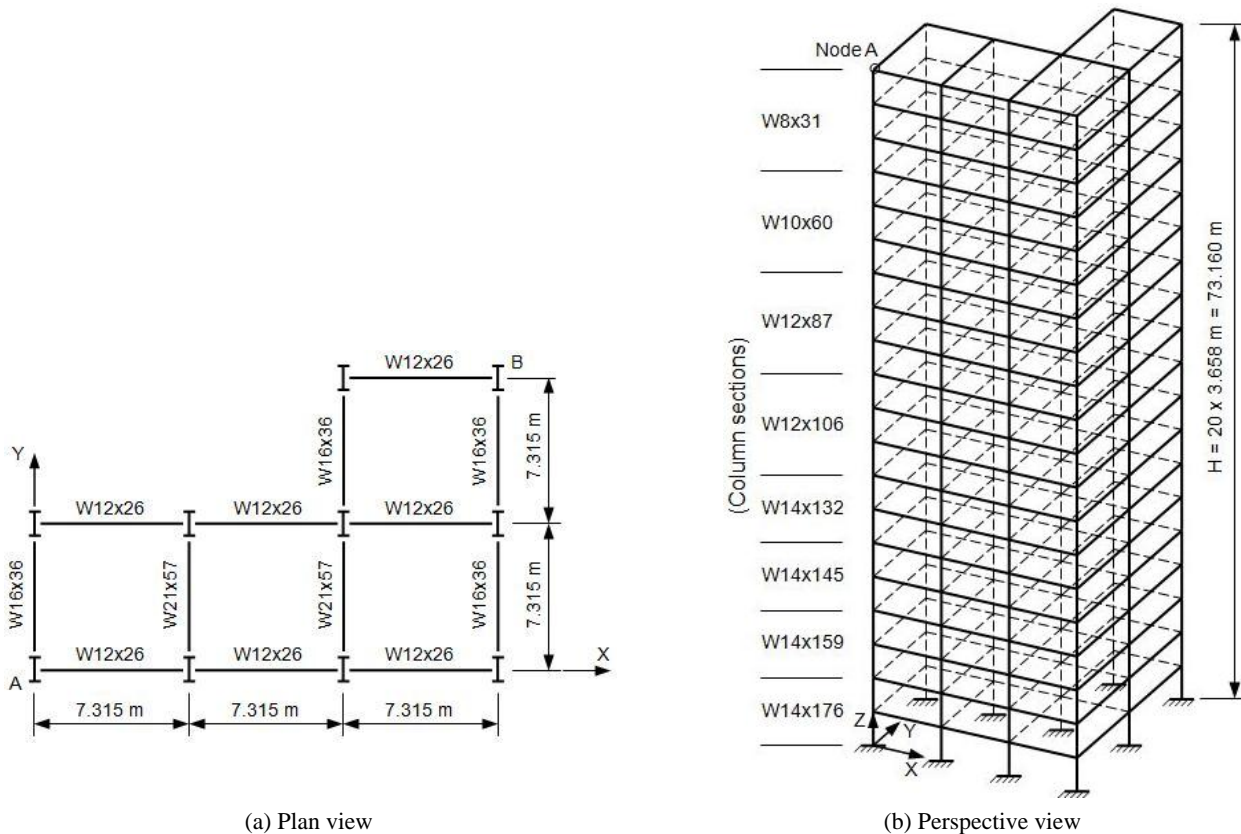


Fig. 10 Twenty-story space frame

inelastic behavior. Chiorean and Barsan employed the inelastic Ramberg-Osgood force-strain relationships to model the gradual yielding of cross-section. In this analysis, one element with seven integration points was used to model each beam-column member and two values of $n = 30$ (corresponding to plastic zone approach) and $n = 300$ (corresponding to plastic hinge approach) for Ramberg-Osgood shape parameters were considered. In the present study, one element per member is used to model the frame, and two analyses are performed: the proposed analysis (LB and LTB considered) and the conventional analysis (LB and LTB ignored).

The load-displacement curves of node A at the roof of the frame obtained by the present study and the others are compared in Fig. 11. The ultimate load factor of the frame is also given in Table 2. It is noted that all sections used in this example are compact which can develop full plastic moment capacity without LB. In the proposed analysis, the structure is collapsed by the LTB at the ultimate load factor of 0.751. In the conventional analysis, the ultimate load factor of the present work (1.021) is close to those of Jiang (1.0) and Chiorean and Barsan using $n = 300$ (1.005), and the load-deflection curves of the present study are similar to those of Chiorean and Barsan using $n = 300$. As a result, the

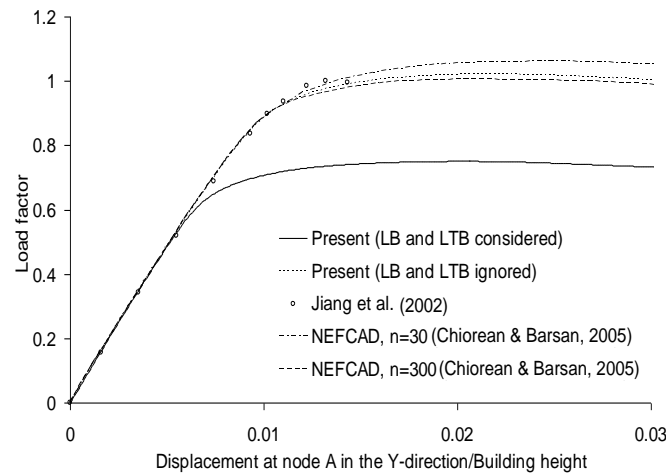


Fig. 11 Load-displacement curves of twenty-story space frame

Table 2 Analysis result of twenty-story space frame

Author	Ultimate load factor
Jiang <i>et al.</i> (2002)	1.000
Chiorean and Barsan (2005), $n = 30$	1.062
Chiorean & Barsan (2005), $n = 300$	1.005
Present (LB and LTB ignored)	1.021
Present (LB and LTB considered)	0.751

conventional analysis overpredicts the load-carrying capacity of the frame by 1.36 times. Using the same personal computer configuration (Pentium III, 500 MHz), the analysis time of the present study lasts only 7 min, while the full spread-of-plasticity and mixed element approaches of Jiang take about 20 h and 1.7 h, respectively, for the same analysis. This example is a good illustration on the accuracy and computational efficiency of the proposed program in predicting the second-order inelastic behavior of the large-scale space frames.

5. Conclusions

The aim of this paper is to improve the refined plastic hinge analysis by accounting for the effects of local buckling and lateral-torsional buckling. The degradation of the flexural strength caused by local buckling and lateral-torsional buckling is implicitly accounted for using the practical LRFD equation. The GDC method is employed to trace the equilibrium path of the nonlinear problems with multiple limit points and snap-back points. As shown in some numerical examples, the proposed analysis shows the capability of predicting accurately and efficiently the second-order inelastic behavior of space frame. It can be concluded that the proposed analysis proves to be reliable and valuable for application in engineering design.

Acknowledgments

This work was supported by the Human Resources Development of the Korea Institute of Energy Technology

Evaluation and Planning (KETEP) grant funded by the Korea government Ministry of Knowledge Economy (No. 20104010100520), and the School of Engineering and Mathematical Sciences at La Trobe University.

References

- AISC-LRFD (1994), Load and resistance factor design specification; AISC, Chicago, IL, USA.
- Argyris, J., Boni, B., Hindenlang, U. and Kleiber, M. (1982), "Finite element analysis of two- and three-dimensional elasto-plastic frames-the natural approach", *Comput. Methods Appl. Mech. Eng.*, **35**(2), 221-248.
- Chiorean, C.G. (2013), "A computer method for nonlinear inelastic analysis of 3D composite steel-concrete frame structures", *Eng. Struct.*, **57**, 125-152.
- Chiorean, C. and Barsan, G. (2005), "Large deflection distributed plasticity analysis of 3D steel frameworks", *Comput. Struct.*, **83**(19), 1555-1571.
- Cichon, C. (1984), "Large displacements in-plane analysis of elastic-plastic frames", *Comput. Struct.*, **19**(5), 737-745.
- De Souza, R.M. (2000), "Force-based finite element for large displacement inelastic analysis of frames", Ph.D. Dissertation; Department of Civil & Environmental Engineering, University of California at Berkeley, CA, USA
- Hoang, V.L. and Nguyen Dang, H. (2008), "Local buckling check according to Eurocode-3 for plastic-hinge analysis of 3-D steel frames", *Eng. Struct.*, **30**(11), 3105-3113.
- Iu, C.K., Bradford, M.A. and Chen, W.F. (2009), "Second-order inelastic analysis of composite framed structures based on the refined plastic hinge method", *Eng. Struct.*, **31**(3), 799-813.
- Jiang, J. and Usmani, A. (2013), "Modeling of steel frame structures in fire using OpenSees", *Comput. Struct.*, **118**, 90-99.
- Jiang, X.M., Chen, H. and Liew, J. (2002), "Spread-of-plasticity analysis of three-dimensional steel frames", *J. Constr. Steel Res.*, **58**(2), 193-212.
- Kim, S.E., Park, M.H. and Choi, S.H. (2001), "Direct design of three-dimensional frames using practical advanced analysis", *Eng. Struct.*, **23**(11), 1491-1502.
- Kim, S.E., Lee, J. and Park, J.S. (2002), "3-D second-order plastic-hinge analysis accounting for lateral torsional buckling", *Int. J. Solids Struct.*, **39**(8), 2109-2128.
- Kim, S.E., Lee, J. and Park, J.S. (2003), "3-D second-order plastic-hinge analysis accounting for local buckling", *Eng. Struct.*, **25**(1), 81-90.

- Landesmann, A. (2012), "Refined plastic-hinge model for analysis of steel-concrete structures exposed to fire", *J. Constr. Steel Res.*, **71**, 202-209.
- Liu, S.-W., Liu, Y.P. and Chan, S.L. (2012), "Advanced analysis of hybrid steel and concrete frames: Part 2: Refined plastic hinge and advanced analysis", *J. Constr. Steel Res.*, **70**, 337-349.
- Mohri, F., Bouzerira, C. and Potier-Ferry, M. (2008), "Lateral buckling of thin-walled beam-column elements under combined axial and bending loads", *Thin-Wall. Struct.*, **46**(3), 290-302.
- Orbison, J.G. (1982), "Nonlinear static analysis of three-dimensional steel frames", Report No. 82-6; Department of Structural Engineering, Cornell University, NY, USA.
- Rigobello, R., Breves Coda, H. and Munaier Neto, J. (2013), "Inelastic analysis of steel frames with a solid-like finite element", *J. Constr. Steel Res.*, **86**, 140-152.
- Teh, L.H. and Clarke, M.J. (1999), "Plastic-zone analysis of 3D steel frames using beam elements", *J. Struct. Eng.*, **125**(11), 1328-1337.
- Thai, H.T. and Choi, D.H. (2013), "Advanced analysis of multi-span suspension bridges", *J. Constr. Steel Res.*, **90**, 29-41.
- Thai, H.T. and Kim, S.E. (2011), "Practical advanced analysis software for nonlinear inelastic dynamic analysis of steel structures", *J. Constr. Steel Res.*, **67**(3), 453-461.
- Torkamani, M.A. and Sonmez, M. (2001), "Inelastic large deflection modeling of beam-columns", *J. Struct. Eng.*, **127**(8), 876-887.
- Yang, Y.B. and Shieh, M.S. (1990), "Solution method for nonlinear problems with multiple critical points", *AIAA Journal*, **28**(12), 2110-2116.
- Zubydan, A.H. (2013), "Inelastic large deflection analysis of space steel frames including H-shaped cross sectional members", *Eng. Struct.*, **48**, 155-165.